A review of focused ion beam applications in microsystem technology

2001 J. Micromech. Microeng. 11 287

(http://iopscience.iop.org/0960-1317/11/4/301)

INSTITUTE OF PHYSICS PUBLISHING JOURNAL OF MICROMECHANICS AND MICROENGINEERING
J. Micromech. Microeng. **11** (2001) 287–300 www.iop.org/Journals/jm PII: S0960-1317(01)18940-0

A review of focused ion beam applications in microsystem technology

Steve Reyntjens and Robert Puers

Katholieke Universiteit Leuven, ESAT-MICAS, K Mercierlaan 94, B-3001 Heverlee, Belgium

E-mail: steve.reyntjens@esat.kuleuven.ac.be and bob.puers@esat.kuleuven.ac.be

Received 12 January 2001

Abstract

In this paper the possibilities of focused ion beam (FIB) applications in microsystem technology are reviewed. After an introduction to the technology and the operating principles of FIB, two classes of applications are described. First the subject of FIB for microsystem technology inspection, metrology and failure analysis is outlined. A procedure for cross sectioning on samples is presented, as well as some examples of how this technique can be applied to study processing results. The second part of the paper is on the use of FIB as a tool for maskless micromachining. Both subtractive (etching) and additive (deposition) techniques are discussed, as well as the combination of FIB implantation of silicon with subsequent wet etching. We will show the possibility to fabricate three-dimensional structures on a micrometre scale, and give examples of recent realizations thereof.

(Some figures in this article are in colour only in the electronic version; see `www.iop.org`)

1. Introduction

The focused ion beam (FIB) technique was mainly developed during the late 1970s and the early 1980s, and the first commercial instruments were introduced more than a decade ago [1]. Modern FIB systems are becoming widely available in semiconductor research and processing environments, as well as in failure analysis and chip-design centres. The technology enables localized milling and deposition of conductors and insulators with high precision, hence its success in device modification, mask repair, process control and failure analysis [2–6]. Also, the preparation of specimens for transmission electron microscopy (TEM) and the trimming of thin-film magnetoresistive heads (for magnetic storage disks) are important applications of FIB, which will be discussed [7, 8]. Only recently, a number of authors have reported the use of FIB in micromachining applications for MEMS [9, 10, 25, 30]. Some promising realizations will be reviewed in this paper.

2. FIB technology

A typical small-footprint FIB system is shown in figure 1. The most important components of the system are indicated: the ion column, the work chamber, the vacuum system and the gas system (not shown) and the workstation that provides the user interface. These subsystems will be discussed in detail in the following paragraphs.

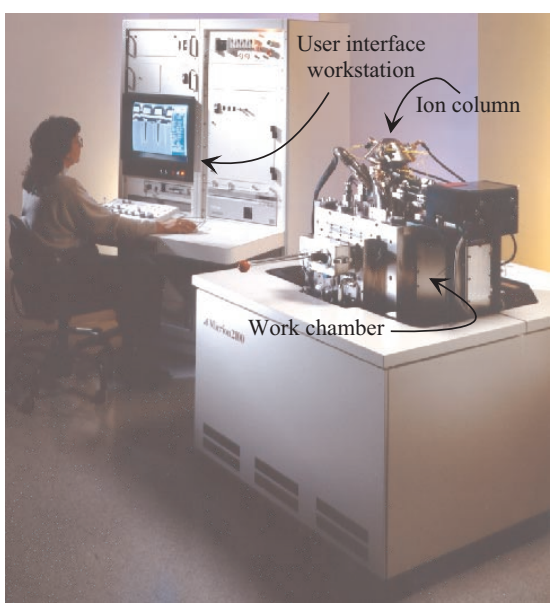

Figure 1. Typical small-footprint FIB system (Micrion 2500). The most important components are indicated on the photograph.

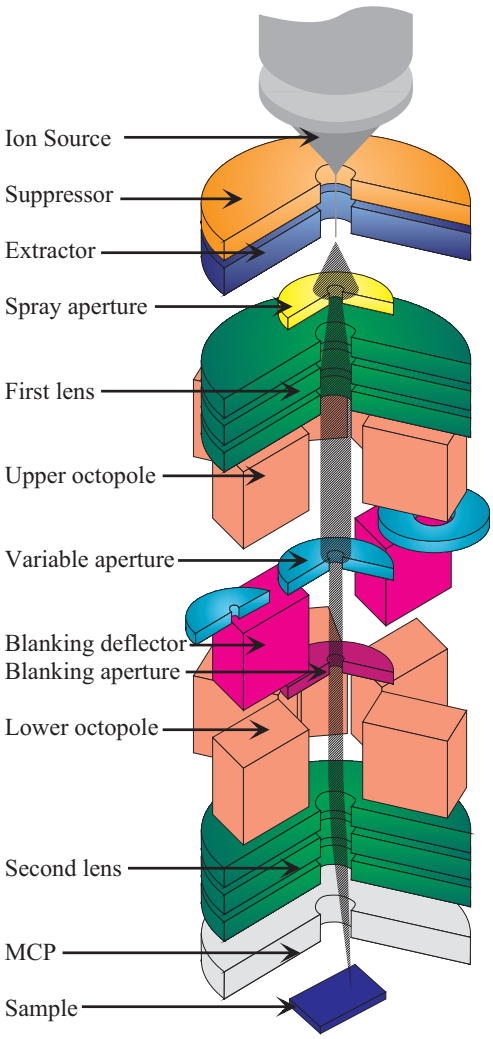

Figure 2. Schematic diagram of a FIB ion column.

2.1. Ion column

A schematic diagram of a FIB ion column is shown in figure 2. The structure of the column is similar to that of a scanning electron microscope, the major difference being the use of a gallium ion (Ga^+) beam instead of an electron beam. A vacuum of about 1×10^{-7} mbar is maintained inside the column.

The ion beam is generated from a liquid-metal ion source (LMIS) by the application of a strong electric field. This electric field causes the emission of positively charged ions from a liquid gallium cone, which is formed on the tip of a tungsten needle. A typical extraction voltage is 7000 V. The extraction current under normal operating conditions is 2 μA.

After a first refinement through the spray aperture, the ion beam is condensed in the first electrostatic lens. The upper octopole then adjusts the beam stigmatism. The ion beam energy is typically between 10 and 50 keV, with beam currents varying between 1 pA and 10 nA. Using the variable aperture mechanism, the beam current can be varied over four decades, allowing both a fine beam for high-resolution imaging on sensitive samples and a heavy beam for fast and rough milling. Typically seven values of beam current can be selected: for example 1 pA, 5 pA, 32 pA, 99 pA, 672 pA, 1.5 nA and 8 nA (exact values depend on the machine type and the users' preferences).

Blanking of the beam is accomplished by the blanking deflector and aperture, while the lower octopole is used for raster scanning the beam over the sample in a user-defined pattern. In the second electrostatic lens, the beam is focused to a fine spot, enabling a best resolution in the sub 10 nm range. The multichannel plate (MCP) is used to collect secondary particles for imaging. The imaging principle is discussed in the following sections.

2.2. Work chamber

The samples that are treated by a FIB are mounted on a motorized five-axis stage, inside the work chamber. Under normal operating conditions, inside this stainless-steel chamber a vacuum in the low 10^{-7} mbar range is maintained. Loading and unloading of the samples is usually done through a loadlock, in order to preserve the vacuum inside the work chamber as much as possible. It typically takes a few minutes to load or unload a sample.

2.3. Vacuum system and gas delivery system

A system of vacuum pumps is needed to maintain the vacuum inside the column and the work chamber. A forepump is used in combination with a turbo pump for pumping the work chamber. The ion column is additionally provided with one or two ion pumps.

On most FIBs, a system is available for delivering a variety of gases to the sample surface. To this end a gas cabinet containing all applicable gases is present outside the vacuum chamber. The gas containers are connected to a so-called nozzle assembly inside the vacuum chamber through an appropriate piping system. The gases are used for faster and more selective etching, as well as for the deposition of materials (see below).

2.4. User interface

All operations such as loading and unloading of samples (partly), manipulating the stage, controlling valves for gas delivery, turning on and off pumps and manipulating the ion beam are carried out via software. Indeed, the complete user interface is realized by means of a computer workstation.

3. Principle of FIB imaging, milling and deposition

When energetic ions hit the surface of a solid sample they lose energy to the electrons of the solid as well as to its atoms. The most important physical effects of incident ions on the substrate are: sputtering of neutral and ionized substrate atoms (this effect enables substrate milling), electron emission (this effect enables imaging, but may cause charging of the sample), displacement of atoms in the solid (induced damage) and emission of phonons (heating). Chemical interactions include the breaking of chemical bonds, thereby dissociating molecules (this effect is exploited during deposition).

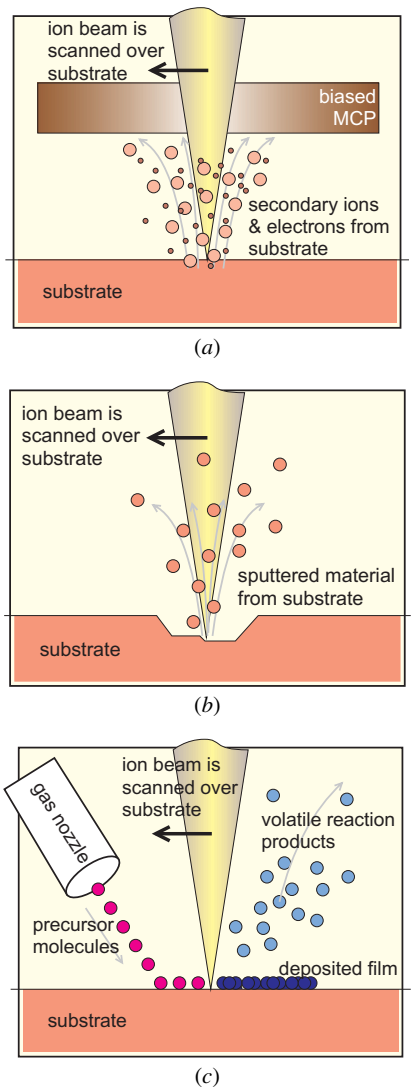

Figure 3. Principle of FIB (*a*) imaging, (*b*) milling and (*c*) deposition.

3.1. Imaging

As illustrated in figure 3(*a*), during FIB imaging the finely focused ion beam is raster scanned over a substrate, and secondary particles (neutral atoms, ions and electrons) are generated in the sample. As they leave the sample, the electrons or ions are collected on a biased detector (a MCP). The detector bias is a positive or a negative voltage, respectively, for collecting secondary electrons or secondary ions. The secondary ions that are emitted can be used for secondary ion mass spectroscopy (SIMS) of the target material in a mass spectrometer attached to the system.

Inevitably, during FIB operations, a small amount of Ga^+ ions are implanted in the sample, and large numbers of secondary electrons leave the sample. To prevent positive surface charges from building up, the substrate can be flooded with electrons from a separate electron source (only when collecting secondary ions for imaging). The system thus prevents damage due to electrostatic discharge and it enables the reliable imaging of non-conducting materials such as glass (which is often used in microsystems).

Figure 4. The beverage can that was cross sectioned for figure 5.

The best resolution of FIB images equals the minimum ion beam spot size, i.e. below 10 nm.

In crystalline materials such as aluminium and copper, the ion penetration depth varies due to channelling along open columns in the lattice structure. Since the secondary electron emission rate depends on the penetration depth, FIB can be used to image crystal grains, revealing different crystal orientations. To illustrate this phenomenon, an aluminium beverage can was cross sectioned, as shown in figure 4. The actual cross sections at different tilting angles are shown in figure 5; the different tilt angles are 30°, 35°, 40° and 45° respectively. The aluminium grains are visible as well as the polymer label on top of the aluminium. The aluminium grains are particularly evident due to channelling contrast. Changing the angle between the ion beam and the sample surface (equivalent to changing the sample tilt angle) causes the grains to be oriented differently with respect to the beam. This manifests itself in the changing brightness of the grains under different tilting angles.

It should be mentioned that imaging with FIB inevitably induces some damage to the sample. Most of the Ga^+ ions that arrive at the sample surface enter the sample; thus ion implantation occurs. The depth of this implanted region is related to the ion energy and the angle of incidence. Typical values for different materials are given in table 1. Besides implantation, some milling always occurs when the ion beam is scanned across the sample surface. Of course this milling effect can be drastically reduced when using a fine ion beam (fine spot and low ion current).

3.2. Milling

The removal of sample material is achieved using a high ion current beam. The result is a physical sputtering of sample material, as illustrated schematically in figure 3(*b*). By scanning the beam over the substrate, an arbitrary shape can be etched. Typical sputtering yield figures for various materials and normal incidence are given in table 1. However, these numbers cannot be used directly to calculate the etch rate, because, depending on the scanning style, redeposition occurs, which drastically reduces the effective etch rate. Furthermore,

Table 1. Typical implantation depth and sputtering yield for Ga^+ ions in silicon (Si), silicon dioxide (SiO_2), aluminium (Al), at normal incidence. The figures in this table were obtained using TRIM Monte Carlo simulations [31].

	Implantation depth (nm)			Sputtering yield (atoms/ion)		
Ga^+ ion energy	Si	SiO_2	Al	Si	SiO_2	Al
10 keV	13 ± 5	12 ± 4	11 ± 4	1.46	Si: 0.62; O: 2.23	2.59
20 keV	20 ± 7	19 ± 6	17 ± 6	1.87	Si: 0.64; O: 2.34	2.98
30 keV	27 ± 9	25 ± 8	23 ± 8	1.98	Si: 0.67; O: 2.25	2.91
40 keV	33 ± 11	31 ± 10	29 ± 10	2.04	Si: 0.77; O: 2.54	3.54
50 keV	39 ± 14	38 ± 11	35 ± 12	2.01	Si: 0.67; O: 2.39	3.48

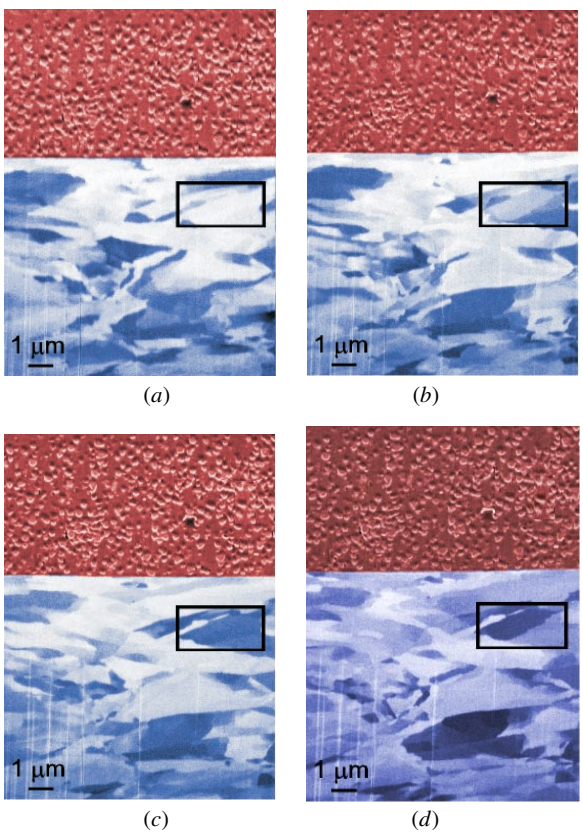

Figure 5. Cross section through an aluminium beverage can, visualized from various tilting angles: (*a*) 30°, (*b*) 35°, (*c*) 40°, and (*d*) 45°. The aluminium grains are clearly visible (lower part), as well as the polymer label (upper part). The tilt angle-dependent channelling contrast is clearly illustrated by the boxed grain.

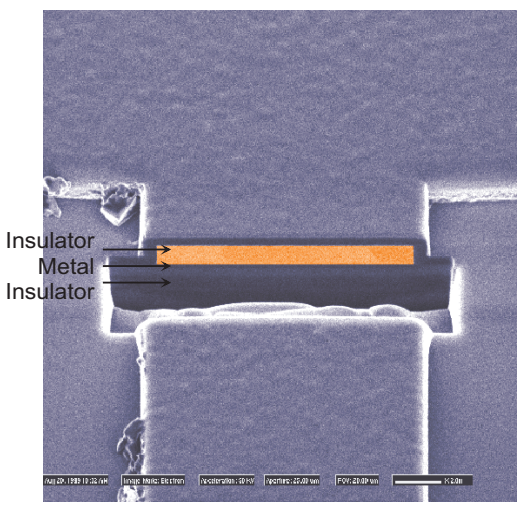

Figure 6. Typical milling example: a metal line is cut to electrically isolate it from the rest of the circuit.

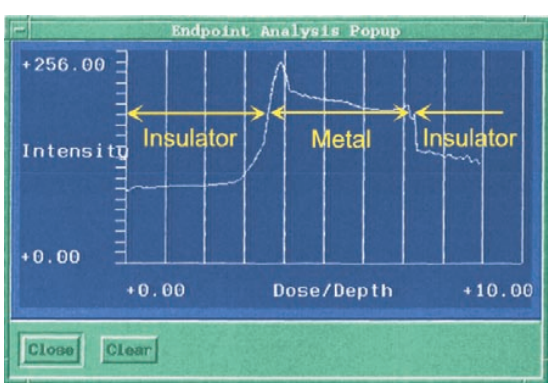

Figure 7. End-point detection. The graph shows the average brightness in the milling area as a function of the delivered dose. This is used to monitor the milling operation in real time. The insulator–metal–insulator stack is clearly recognized.

the sputtering yield is dependent on the angle of incidence: it roughly increases with $1/\cos(\theta)$, with θ the angle between the surface normal and the ion beam direction.

In figure 6, a typical milling example is shown. A metal conductor is cut by milling a rectangle through it. In this way, the electrical connection is removed. The milling process is monitored through the 'end-point detection'; this is a real-time graph of the average brightness in the milling area. An insulator will appear darker than a conductor since the secondary electron yield of the latter is much higher. This effect results in a typical end-point detection curve as shown in figure 7. The first part (low brightness) corresponds to the insulating dielectric layer over the metal conductor. The metal itself is the central high-intensity part. Finally, after milling through the metal, the intensity diminishes again when the underlying insulating layer is reached. This information is used to detect the complete removal of the metal layer. The resolution of the milling process is a few tens of nanometres. The typical maximum aspect ratio of the milled holes is 10–20.

In order to speed up the milling process, or to increase the selectivity towards different materials, an etching gas can be introduced into the work chamber during milling. It will increase the etching rate and the selectivity towards different

materials by chemically facilitating the removal of reaction products. This technique is called gas-assisted etching (GAE). Typical etching gases and their the milling rate enhancement factors are shown in table 2.

3.3. Deposition

FIB enables the localized maskless deposition of both metal and insulator materials. The principle is chemical vapour deposition (CVD) and the occurring reactions are comparable to, for example, laser induced CVD [11, 12]. The main difference is the better resolution but lower deposition rate of FIB.

The metals that can be deposited on commercially available machines are platinum (Pt) and tungsten (W). In the case of W, the organometallic precursor gas is $W(CO)_6$. The deposited insulator material is SiO_2, with 1, 3, 5, 7-tetramethylcyclotetrasiloxane (TMCTS) and oxygen (O_2) (or alternatively water vapour (H_2O)) as precursors.

The deposition process is illustrated in figure 3(*c*); the precursor gases are sprayed on the surface by a fine needle (nozzle), where they adsorb. In a second step, the incending ion beam decomposes the adsorbed precursor gases. Then the volatile reaction products desorb from the surface and are removed through the vacuum system, while the desired reaction products (W or SiO_2) remain fixed on the surface as a thin film. The deposited material is not fully pure however, because organic contaminants as well as Ga^+ ions (from the ion beam) are inevitably included.

In figure 8(*a*), a simple metal deposition example is shown. It is a thin tungsten line, 10 μm wide, on top of an oxidized Ti cylinder with diameter of about 3.5 mm. It is important to stress that FIB processing is as convenient on non-planar surfaces (such as this cylinder) as it is on traditional flat surfaces. In figure 8(*b*), a thick SiO_2 deposition is shown. The deposition has a bitmapped shape instead of a simple rectangle.

The smallest features that can be deposited are of the order of 100 nm (lateral dimension). The minimal thickness is about 10 nm. Aspect ratios between 5 and 10 are obtained, at a typical deposition rate of 0.05 $\mu m^3\ s^{-1}$.

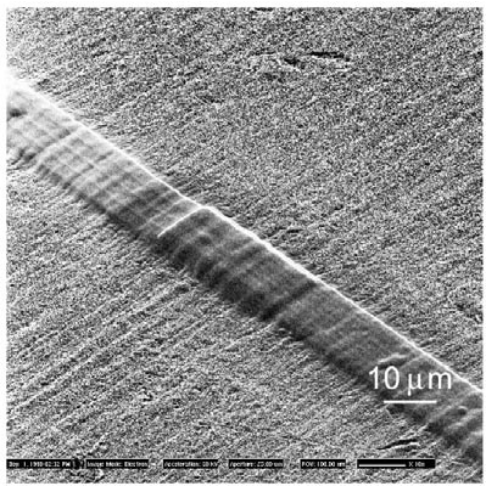

(*a*)

(*b*)

Figure 8. Deposition examples: (*a*) a 10 μm wide tungsten line on a cylindrical surface and (*b*) a 3.3 μm thick SiO_2 deposition in a bitmap shape.

4. FIB as a microtechnology inspection and metrology tool

Among the most successful applications of FIB in semiconductor technology is failure analysis. In addition, for microsystems, a lot of information can be gained from careful inspection of processed structures. In particular, the cross sectioning capability has proven to be very valuable for microsystems.

The most remarkable merit of FIB for technology inspection and metrology is its flexibility. It is very easy to work on individual dies as well as on entire wafers. On the smaller machines the wafer size is limited to 75 mm, while on the larger machines wafers up to 200 mm can be treated. Furthermore, it is also possible to work on packaged devices.

The flexibility of processing scale is a consequence of the inherent advantage of FIB: it always processes locally. This enables to (destructively) test or check dimensions on just one or a few dies on a wafer. The unaffected dies on the rest of the wafer can then continue the rest of the normal process. This enables intermediate inspection of, for example, process tolerances, whilst minimizing the loss of good dies.

Practically any material can be milled and visualized, including non-conducting materials (in ion mode). Non-conducting surfaces do not need a special pretreatment (metal coating) as is the case for scanning electron microscopy (SEM) inspection. In terms of deposition, the range of materials that is commercially available is rather limited however. Standard machines have tungsten or platinum as metals (conductors) and silicon dioxide as an insulator material. However, a wider range of other materials have already been deposited in research laboratories (e.g. Ta [2], Au [13, 15], C [13], Fe [14], Al [14]), and new materials for deposition are being developed. The near future of silicon technology will be characterized by the widespread introduction of new materials such as copper, polymer-based low-K dielectrics and new gate materials. Integrating these materials will require new types of gases for selective etching and deposition with FIB [16].

Finally, there is flexibility in the working dimensions in FIB: accurate imaging, milling and deposition are feasible on a scale ranging from a few tens of nanometres to hundreds of micrometres. The possibility to change the ion beam current over four decades is the main factor enabling this large variation of processing sizes, accuracy and speed.

Table 2. Typical GAE gases and their etch rate enhancement factors on various materials.

	Aluminium	Tungsten	Silicon	SiO_2, Si_3N_4	Photoresist, polyimide
Cl_2	10–20	—	10	—	—
Br_2	10–20	—	6–10	—	—
ICl	8–10	2–6	4–5	—	—
XeF_2	—	10	10–100	6–10	3–5

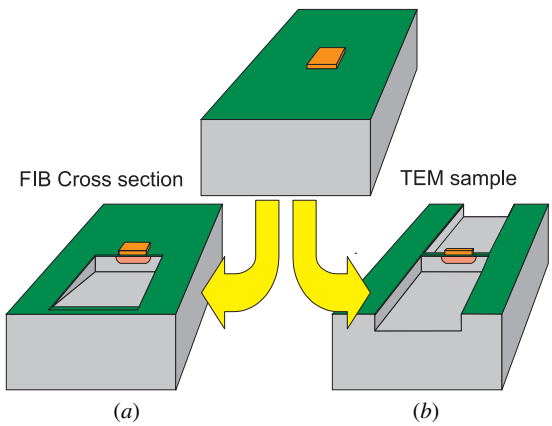

Figure 9. Sample with feature of interest can be (*a*) cross sectioned in the FIB. The section can be advanced until desired feature appears or (*b*) it can be prepared for inspection in a TEM.

The benefits of FIB are fully exploited in the cross sectioning technique, which will be dealt with in the following sections.

4.1. Cross sectioning procedure

For the cross sectioning of samples, the use of FIB offers several advantages over other techniques. While cleaving or dicing and polishing for SEM investigations take several hours, FIB enables cross sections to be realized within a few minutes time. Furthermore, one is free to determine the precise location of the cross section, and an arbitrary number of subsequent cross section 'slices' can be taken on the same sample.

The principle of the cross sectioning technique is illustrated in figure 9(*a*). In a first step, adjacent to the location of interest, bulk material is removed with a rough and fast single-pass mill. This results in a steep sidewall on the side near the feature of interest. This sidewall is made perfectly vertical and is smoothly polished in the subsequent milling step(s), using each time a finer ion beam and milling regime (polish mill) (this is illustrated in more detail in the first example, see figure 11). Finally the sample is tilted, and the polished sidewall is visualized. For normal cross sections (depth of a few micrometres and width 10–15 μm), the whole procedure takes no more than 15 min.

In the following sections, we will give some examples of how this technique can be used for analysing real microstructures. It is also possible to use a similar technique on both sides of the region of interest. This then enables one to fabricate a thin lamella, suited for inspection by TEM. The principle of this technique is illustrated in figure 9(*b*). More details are given in section 5, on micromachining.

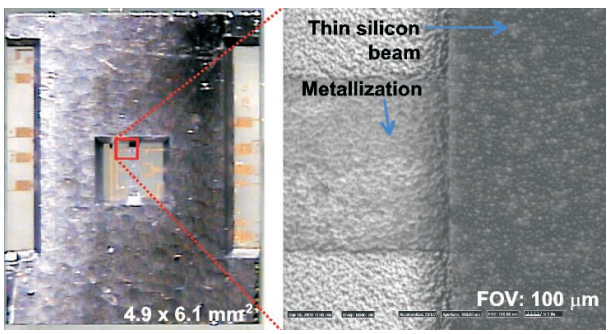

Figure 10. Autonomous switched resonator: chip overview and surroundings of the cross section.

4.1.1. Example 1: autonomous switched resonator: evaluation of the technological process. The autonomous switched resonator [18] is a glass–silicon stacked structure. In figure 10, the overall structure is shown: on a glass substrate, a silicon chip is bonded. The chip has an etched window that carries a long thin beam. This beam can be electrostatically attracted to the glass by means of Pt electrodes. Between the electrodes, a small gap is present. In figure 11(*a*), the exact location of the cross section is indicated. As explained above, the milling starts with a single-pass mill, which removes most of the bulk material. The result after this milling step is shown in figure 11(*b*). Then the vertical sidewall containing the feature of interest is made straight and smooth with a polish mill, the result of which is shown in figure 11(*c*).

The sample is now tilted to typically 45° or 60° with respect to the ion beam, and a high resolution image is acquired. The result is shown in figure 12. From bottom to top, the following elements are clearly visible: the platinum electrode on the glass, the platinum electrode on the silicon, the thin SiO_2 layer and the silicon beam (notice the severe sidewall curvature due to underetching).

All layer thicknesses and lateral dimensions can accurately be determined in an easy and straightforward way from this cross section.

4.1.2. Example 2: thick copper conductors: metrology. For an intraocular telemetric pressure sensor, silicon chips with coils were realized in the MICAS laboratory [17]. In order to realize a low resistance (thus a high quality factor), the inductor is fabricated in electroplated copper, using a thick photoresist as a mask. The AZ4562 resist (Hoechst) is suitable for conventional UV lithography, and enables the development of relatively high aspect ratio structures. During the fabrication process, FIB is used at intermediate stages to check and measure the dimensions and shapes of the realized structures.

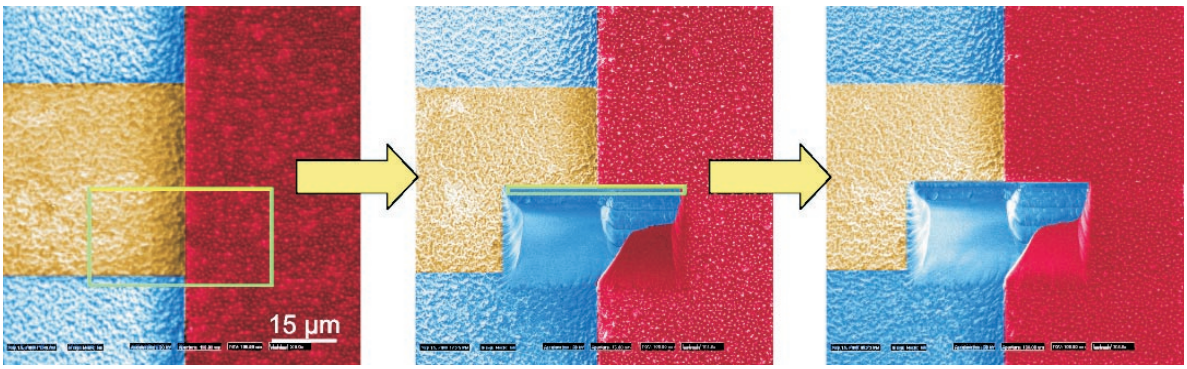

Figure 11. Resonator close-up: (*a*) the starting situation, (*b*) after a single-pass mill and (*c*) after a polish mill.

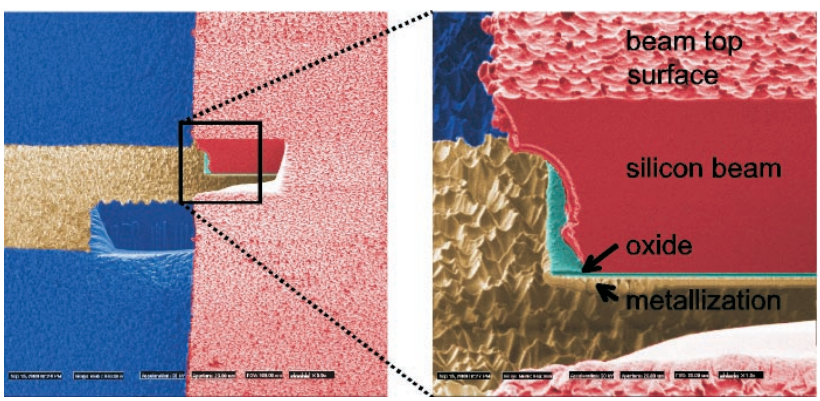

Figure 12. The cross sectioned face on the tilted resonator (60°); as well as some further detail.

An overview of the fabrication process is given in figure 13. The stages where a FIB cross section is taken, are indicated by the dotted rectangles. The process shown in figure 13 can be described as follows: figure 13(*a*), growth of 600 nm of SiO_2 on the silicon substrate and sputtering of a 50 nm Ti/100 nm Cu seed layer; figure 13(*b*), spinning, softbake, illumination, development and hardbake of 12 μm thick resist. A FIB cross section showing the resist profile and dimensions is shown in figure 14(*a*). Note the (dark) oxide layer, and the (bright) Ti/Cu seed layer. Thickness measurements on this cross section allow for dimensional process control. The sidewall shape of the resist is clearly visualized. Figure 13(*c*) shows copper electrodeposition, filling the resist patterns to a height of 9–10 μm. Figure 13(*d*) shows removal of the resist and figure 13(*e*) etching of the seed layer. A FIB cross section showing the dimensions and profile of the copper track as well as a small resist residue on the side is shown in figure 14(*b*). Note the copper grain contrast, enabling an estimate of the copper grain size.

Again all thicknesses, as well as lateral dimensions can be accurately determined in an easy and straightforward way. One inspection sequence (cross sectioning and actual inspection) takes about 30 min, and is non-destructive for adjacent devices on the same wafer.

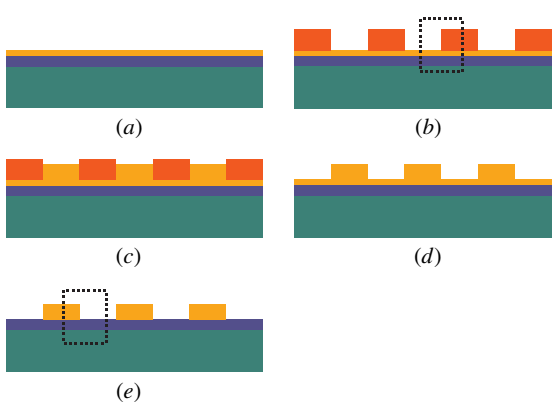

Figure 13. Process sequence of the copper electroplated coils described in the text.

5. FIB as a direct-write micromachining processing tool

A direct-write technique, the high resolution of FIB in combination with a five-axis motorized stage and the possibility to mill and deposit materials yield a powerful tool for maskless micromachining. It should be noted that both subtractive (milling) and additive (deposition) machining are possible in the same machine.

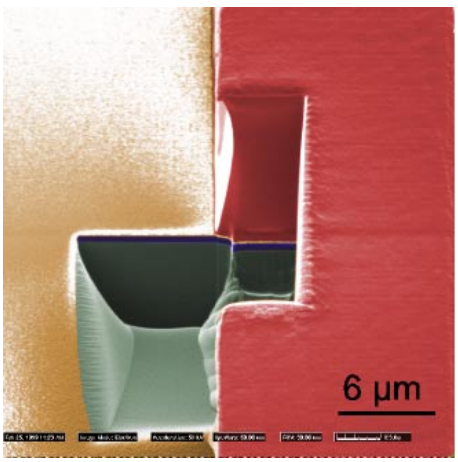

(*a*)

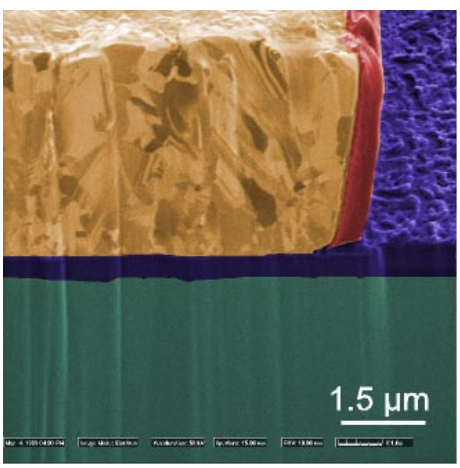

(*b*)

Figure 14. Cross sections for process evaluation during the processing of thick copper coils: (*a*) thick photoresist profile and (*b*) electroplated copper.

In table 3, some common direct-write micromachining techniques are compared. FIB deposition is compared to LCVD and micro stereolithography; FIB milling is compared to laser ablation and microelectrodischarge machining (MEDM). Depending on the application, FIB compares very favourably to other direct-write micromachining techniques, especially in terms of resolution and accuracy. Its main limitation however, is the processing time involved to machine large structures: it is clear that the FIB deposition and etching rates are low. Dimensions up to some tens of micrometres are easily feasible, but above 100 μm, the typical processing times become unacceptably high, and its better to use other (less accurate) techniques.

5.1. Milling

Promising work concerning FIB milling for micromachining applications has been published. Examples are: tunnelling gap milling [27], channel and cantilever milling [24], trimming of magnetoresistive heads [8], TEM membrane preparation [7, 23, 24] and micromachining of Si nanomechanical elements [10].

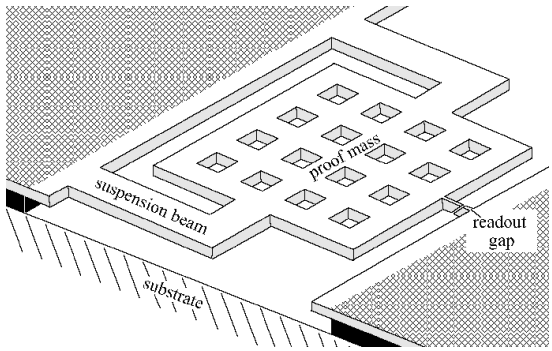

Figure 15. Schematic diagram of the tunnelling accelerometer structure. (Courtesy D F Moore *et al*, Department of Engineering, University of Cambridge [9].)

5.1.1. Tunnelling gap milling on a microaccelerometer. A nice demonstration of the flexibility and accuracy of FIB milling was reported by Daniel [9] and Daniel and Moore [27]. This shows how FIB can be used for a small but highly accurate post-processing step on a micromechanical device. In these papers, a microaccelerometer, fabricated from a silicon-on-insulator (SOI) substrate is described. The short FIB processing step involves cutting a narrow gap obliquely in a silicon beam. This gap is used for reading out an acceleration.

The accelerometer structure is shown schematically in figure 15. The square proof mass is suspended by two suspension beams, and the narrow readout gap is situated in a small silicon beam at the moving end of the proof mass. When the proof mass moves up or down due to an acceleration, the width of the readout gap changes. This change of gap size is monitored (by tunnelling current measurement or duty cycle measurement in a 'tapping mode'—see [9]) and is proportional to the applied acceleration.

In order to keep the FIB milling time per device low, a two-step process is used. The silicon beam is first milled with a high-current ion beam, creating a coarse trench. Then the final part of the gap is milled with a lower current ion beam, i.e. a finely focused beam. This second mill precisely defines the width of the readout gap. The result is a 0.4 μm wide gap at an angle of 45° (figure 16). A total milling time of less than 2 min per device is reported.

5.1.2. TEM sample preparation. TEM sample preparation is an important application of FIB micromachining. To properly use TEM, the samples must be thin enough to transmit an electron beam, typically 100 nm or less.

The traditional preparation procedure is a time consuming and tedious process: once the defective area is located, it is cut from the wafer. This obviously destroys the entire wafer. The sample then undergoes several grinding and polishing steps until both sides, approach the defect. Finally, broad-beam ion milling thins the sample until it is transparent to electrons. The only way to monitor the thinning processes is to frequently move the sample to an optical microscope and inspect it. Many defects are nearly invisible until revealed by the polishing process, and the slightest misjudgment in polishing or ion milling can destroy the sample. Furthermore, soft materials in the sample will smear due to the polishing process.

Table 3. Comparison of some common direct-write micromachining techniques.

Technique	Three-dimensional geometries	Typical maximum aspect ratio	Typical feature sizes	Typical deposition/ etch rate
FIB deposition	+	10	200 nm–20 μm	0.05 $\mu m^3\ s^{-1}$
LCVD [19]	0	1	10 μm–1 mm	100 $\mu m^3\ s^{-1}$
Micro stereolithography [20]	++	n/a	5 μm–5 mm	100 $\mu m^3\ s^{-1}$
FIB milling	+	15	50 nm–50 μm	1 $\mu m^3\ s^{-1}$
Laser ablation [21]	+	5	5 μm–5 mm	500 $\mu m^3\ s^{-1}$
Micro electrodischarge machining [22]	++	10	100 μm–1 mm	100 000 $\mu m^3\ s^{-1}$

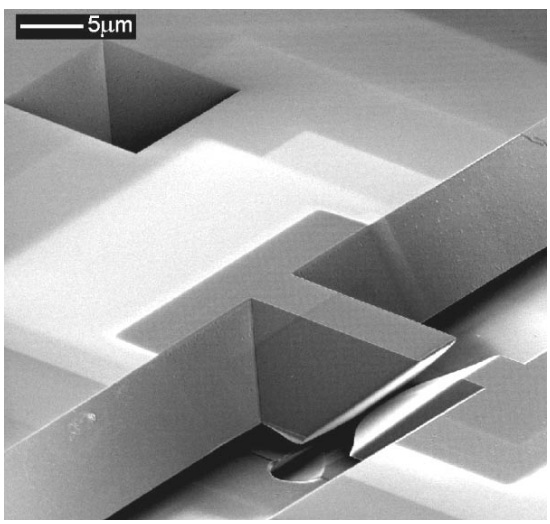

Figure 16. The readout gap milled by FIB. (Courtesy D F Moore *et al*, Department of Engineering, University of Cambridge, [9].)

FIB preparation uses the ion beam to image the sample and to remove material from both sides of the desired section. It will also 'polish' the sample to make it transparent to electrons. In the FIB, material removal is monitored in real time. Two approaches to FIB sample preparation are used nowadays: prethinning [7, 23, 24] or lift out [28].

Prethinning uses traditional mechanical methods to cut a small sample from a wafer and to then thin it to about 10–50 μm. After this, the sample is placed in the FIB. The ion beam removes material from both sides of the desired section using successively lower ion beam currents, leaving a thin membrane for TEM examination. The main advantage is a very accurate positioning of the TEM slice; the sample can even be returned to the FIB for further thinning if needed.

For the lift-out approach, the intact wafer or device is placed in the FIB. Trenches on both sides of the target are milled, using successively lower ion beam currents as in the prethinning technique. When the target reaches a thickness of about 0.5 μm, the wafer is tilted and the target is cut free along its bottom and one side. After further thinning, the remaining side is also cut. The sample, 10–20 μm in length and width and less than 100 nm thick, is lifted out using a fine glass probe and mounted on a TEM grid. Obviously, this approach leaves the remainder of the wafer intact. Also, a lift-out sample requires less material removal, and thus less FIB processing time. An example of a prepared TEM slice before lift-out is shown in figure 17.

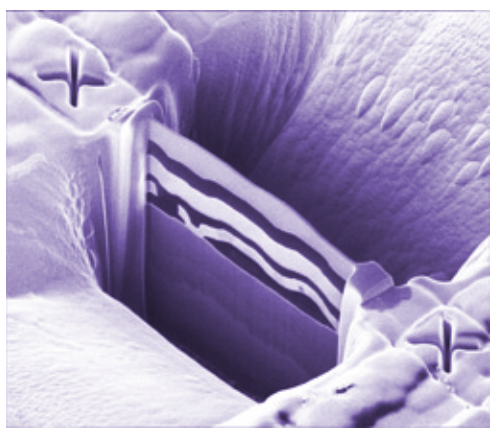

Figure 17. FIB prepared TEM sample.

As mentioned before, one should be aware that FIB processes induce some damage in the samples. The expected damage caused by the ion beam includes implantation of gallium ions, amorphization of crystalline structures, mixing of components and loss of fine structural detail. To prevent top-surface damage, one may deposit a layer of platinum or other metal using an FIB instrument prior to the start of any milling (using low-energy ions!).

5.1.3. Magnetic head trimming. An industrial use of FIB micromachining is trimming and shaping of thin-film magnetic disk heads [8]. FIB milling is used to reduce the pole width of (giant) magneto resistive ((G)MR) heads to 100 nm, thereby increasing the magnetic resolution of the heads (up to areal densities of 100 Gb in^{-2}). FIB vendors offer dedicated machines for magnetic head trimming. The main advantage is that the existing production infrastructure can be maintained, while drastically reducing the critical dimension. The process is fully automated, enabling trimming magnetic heads on wafers and lapped rowbars, through the use of pattern recognition software. Typical cycle times are between 2 and 5 s/head. An example of a FIB trimmed thin-film magnetic head is shown in figure 18.

5.2. Implantation

Brugger *et al* [10] and Schmid *et al* [26] have reported the use of FIB for the implantation of Ga^+ ions with subsequent wet etching. This method is used to fabricate micro- and nanomechanical elements in silicon. It is well known that a high concentration p^+ doping in Si drastically reduces the

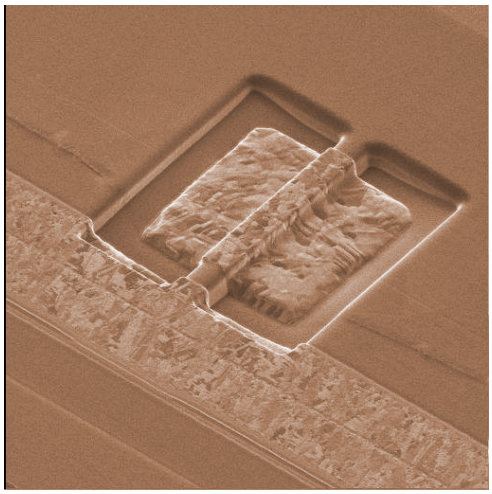

Figure 18. FIB trimmed thin-film magnetic head.

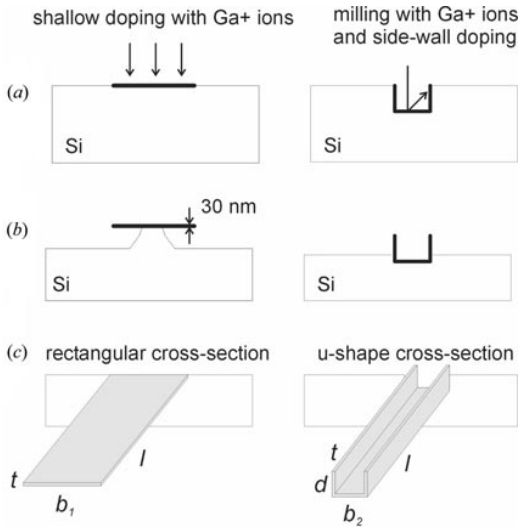

Figure 19. Fabrication of cantilevers by shallow doping (left-hand side) and milling and sidewall doping (right-hand side): (*a*) FIB exposure (milling and/or implantation), (*b*) during KOH etching and (*c*) after etching is completed. (Courtesy N F de Rooij *et al*, Institute of Microtechnology, University of Neuchatel [10].)

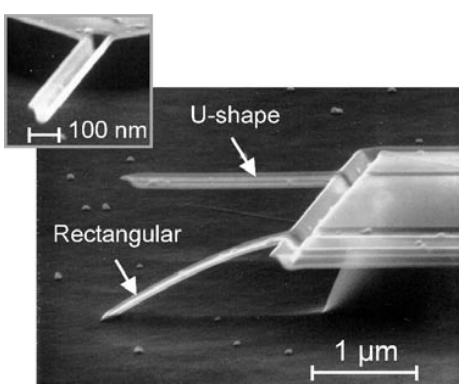

Figure 20. SEM photomicrographs of cantilevers (2 μm long, 100 nm wide and 30 nm thick). (Courtesy N F de Rooij *et al*, Institute of Microtechnology, University of Neuchatel [10].)

etch rate of certain etchants such as potassium hydroxide (KOH) in the implanted region [29]. As the FIB ion energy is typically between 10 and 50 keV, very shallow implanted layers are obtained (shallower than 50 nm). It is found that the critical dose, for the etch stop to be effective, is about 1×10^{15} ions cm^{-2}. Using moderate beam currents (typically 100 pA), this dose is obtained in only a few seconds time on small areas (e.g. 10×10 μm^2). It should be noted that the implanted regions are completely amorphous, considering the amorphization dose of 1×10^{14} ions cm^{-2}. Additionally, for doses above 1×10^{16} ions cm^{-2}, sputtering of the sample surface must be taken into account. This effect can be exploited to realize three-dimensional features.

Cantilevers can be fabricated with a thickness of 30 nm (determined by the implanation depth, which is limited by the ion energy; 30 keV in this case). Their length and width range from 0.5 to 10 μm and from 0.1 to 1 μm, respectively. Figure 19 shows a schematic representations of the two types of cantilevers that were realized: freestanding cantilevers with a rectangular cross section fabricated by shallow doping (left-hand side), and U-shaped cross section cantilevers fabricated by milling and sidewall doping (right-hand side). Figure 20 shows a SEM photomicrograph of the realized devices.

By extending the vertical FIB milling to several micrometres, devices with vertical sidewalls of 30 nm thickness can be fabricated. Doing so, nanocups are fabricated by milling a 200 nm diameter and a few micrometre deep hole in silicon. Subsequent etching yields nanocups with ultrasmall volumes of about 3×10^{-8} nl, as shown in figure 21.

5.3. Deposition

5.3.1. Three-dimensional and overhanging depositions. FIB deposition enables the deposition of complex three-dimensional shapes with overhanging features [30]. The key to this technique is the possibility to deposit features that extend beyond the already present or previously deposited structure underneath. In this way an 'overhang' is created. As the deposition proceeds layer by layer, in each pass the new material extends a bit more over the previously deposited layer. Various three-dimensional structures have been fabricated using this technique, two examples of which are shown in figure 22.

For the overhanging depositions, a clear trade-off exists between accuracy and cleanliness on the one hand, and processing time on the other hand. If a very fine (i.e. low-current) ion beam and a very small overlap between the deposited layers are used, a very accurate deposition is obtained with little or no debris underneath the overhanging parts. On the other hand, if high deposition rates are required, a higher-current ion beam is preferred, which will result in a coarser definition of the deposition pattern and a larger amount of debris. This is illustrated in figure 23, which shows a number of similar depositions with different beam and overlap parameters. Also, the required deposition times differ, although for these small-area depositions the difference is very small. For a 20×20 μm^2 structure, for instance, the difference in deposition time is seven-fold (10 min for 672 pA against 1 h 10 min for 99 pA of ion current).

Table 4. Deposition parameters of the 5 × 2 μm^2 silica blocks shown in figure 23.

Deposition (see figure 23)	Number of boxes	Shift between boxes (μm)	Dose per box (nC μm^{-2})	Ion current (pA)	Total deposition (min, s)
(*a*)	5	0.5	1	672	25, 00
(*b*)	12	0.2	0.4	672	27, 40
(*c*)	5	0.5	1	99	25, 00
(*d*)	12	0.2	0.4	99	27, 40
(*e*)	25	0.1	0.2	99	32, 55

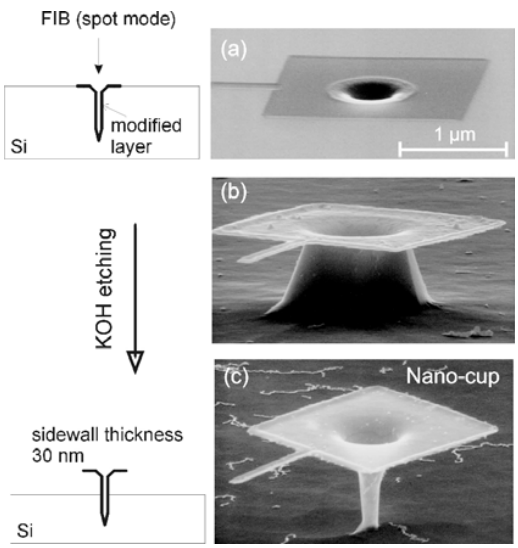

Figure 21. Process sequence for a nanocup: (*a*) after FIB milling a hole, (*b*) after 10 and (*c*) 15 min of KOH etching. (Courtesy N F de Rooij *et al*, Institute of Microtechnology, University of Neuchatel [10].)

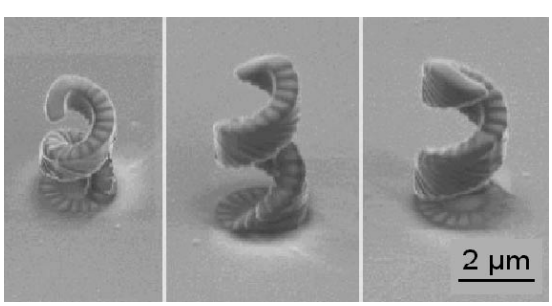

(*a*)

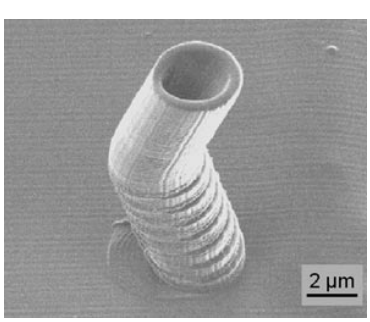

(*b*)

Figure 22. Examples of three-dimensional shaped depositions with overhanging features.

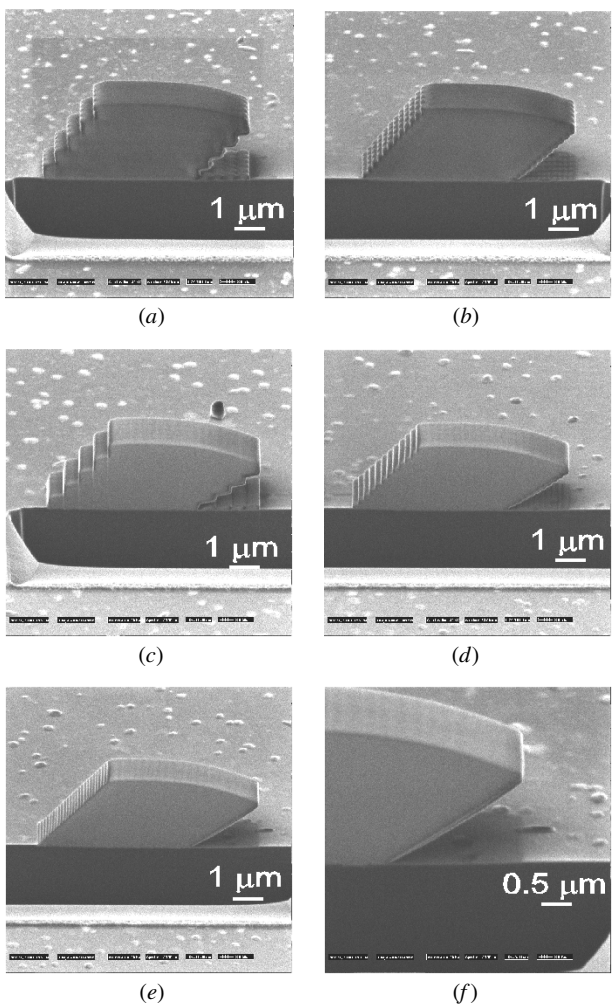

Figure 23. Illustration of the trade-off between speed and accuracy/cleanliness. Cross sections of 5 × 2 μm^2 silica blocks with an overhang, with the deposition parameters given in table 4.

5.3.2. Hermetic encapsulation using FIB deposition. The possibility to fabricate extending or overhanging features is used for the deposition of 'roof'-like structures [25]. As illustrated schematically in figure 24, such a roof structure can be used to encapsulate, for example, a resonating beam. A series of rectangles with steadily decreasing dimensions is deposited, to create a cover. This procedure is illustrated schematically in figure 25, while a typical deposition result is shown in figure 26. The encapsulation deposition is typically performed at a pressure below 5 × 10^{-6} mbar. Therefore, on the inside of the encapsulation, this low pressure is present.

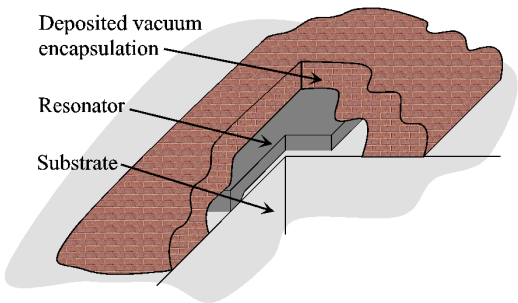

Figure 24. The principle of encapsulation.

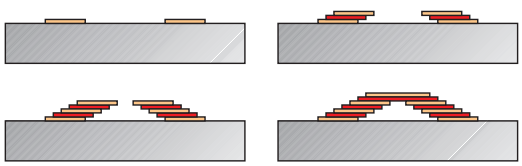

Figure 25. Schematic overview of the deposition process.

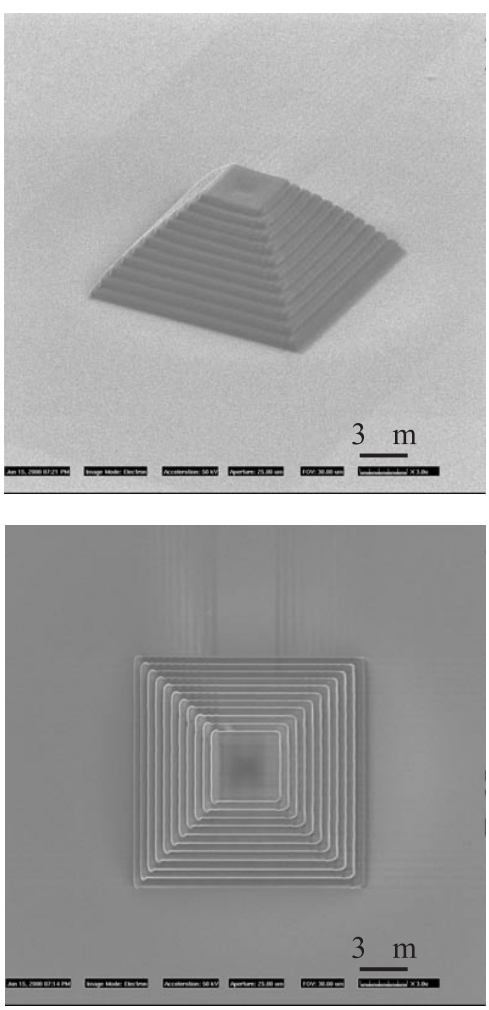

Figure 26. Finished encapsulation deposition. The width of the pyramid is 14 μm, its height is 5 μm.

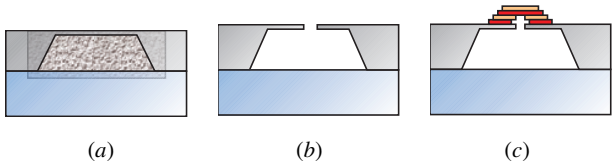

Figure 27. Structure used for the hermiticity test: (*a*) the original glass–silicon stack (with air at atmospheric pressure inside the cavity), (*b*) with a perforated membrane and (*c*) with an evacuated and sealed cavity.

The hermiticity of this type of encapsulation is verified along standard MIL-STD-883 which has as purpose '... to determine ... the hermiticity of the seal of microelectronic devices with internal cavities which are evacuated ...'. The test offers a criterion to decide wether an evacuated cavity can be considered hermetically sealed or not. In order to perform the test, a glass–silicon stack with a thin membrane is fabricated (figure 27(*a*)). The membrane is perforated using FIB milling (figure 27(*b*)), and afterwards the hole is covered by a pyramidal FIB encapsulation (figure 27(*c*)), as described above. After encapsulation the test structure is placed in a sealed chamber which is pressurized with a tracer gas (He at 5 bar). In case of a defect in the seal, the tracer gas is forced into the cavity. After 2 h the pressure is relieved, and the test sample is transferred to another chamber which is connected to a mass spectrometer type leak detector. Any tracer gas which was previously forced into the cavity will thus be drawn out and indicated by the leak detector. The measurements show tracer gas flows that are about an order of magnitude lower than that allowed by the standard. We conclude that the vacuum sealing method using FIB deposition of silica produces hermetic sealing.

An interesting application of this technique is the transformation of a trapped gas pressure sensor into an absolute pressure sensor. As a test device, a piezoresistive bulk micromachined device is used (figure 28(*a*)). The sensor membrane is first perforated using FIB milling. Afterwards this hole is covered again, using the FIB encapsulation technique (figure 28(*b*) shows the sensor after FIB treatment). The sensor is sealed under a vacuum of about 5×10^{-6} mbar, i.e. the pressure at which the deposition of SiO_2 is carried out. This means that on one side of the membrane a vacuum is present, which serves as an absolute pressure reference. Measurements show that the sensor retains its full functionality after FIB processing, and that it still performs as expected after exposure to atmospheric pressure since it was encapsulated (i.e. a period of four months at present).

6. Conclusions and future trends

In this contribution, it is shown that FIB is a powerful tool for the inspection of microsystem technology. It is relatively fast, and works on single dies as well as on entire wafers. The power of this approach lies in its versatility: virtually any material type can be milled and visualized in a flexible way, down to a submicrometre scale. Moreover, it is a non-destructive method if seen on a wafer scale. This enables the inspection of most microsystems of the present day and future.

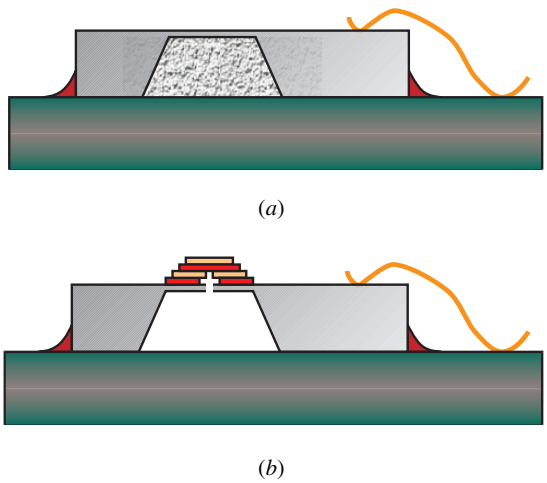

Figure 28. Schematic cross section of a piezoresistive bulk micromachined pressure sensor (*a*) in its original state, as a 'trapped gas' sensor, and (*b*) in its processed state, as an absolute pressure sensor.

Furthermore, it is shown that FIB milling, implantation and deposition offer unique and powerful techniques for the fabrication of three-dimensional microstructures. The hermiticity of FIB deposited encapsulations is demonstrated, and, as an application example, the effortless conversion of a trapped gas sensor into an absolute pressure sensor is reported.

The main benefits of FIB micromachining are the high flexibility in the shapes that can be realized, and the attainable resolution (below 100 nm for deposition, even lower for milling and implantation). The size of the structures that can be obtained is limited by the available processing time. The slow processing is the main drawback of FIB. Hence only relatively small structures (typically tens of micrometres) can be realized within a reasonable time. The technique is best suited for small-scale post-processing or prototype fabrication. Still, it is expected that the technique will seriously expand the frontiers of what is achievable in micromachining in the coming decade.

Acknowledgments

This work is sponsored by the Belgian programme on interuniversity poles of attraction (IUAP 4-24) initiated by the Belgian State, Prime Ministers Office, Science Policy Programming.

References

[1] Melngailis J 1987 Critical review: focused ion beam technology and applications *J. Vac. Sci. Technol.* B **5** 469
[2] Stewart D K, Doyle A F and Casey J D Jr 1995 Focused ion beam deposition of new materials: dielectric films for device modification and mask repair, and Ta films for x-ray mask repair *Proc. SPIE* **2437** 276
[3] Reyntjens S, De Bruyker D and Puers R 1998 Focused ion beam as an inspection tool for microsystem technology *Proc. 1998 Microsystem Symp. (Delft, the Netherlands)* p 125
[4] Ward B W, Economou N P, Shaver D C, Ivory J E, Ward M L and Stern L A 1988 Microcircuit modification using focused ion beams *Proc. SPIE* **923** 92
[5] Glanville J 1989 Focused ion beam technology for integrated circuit modification *Solid State Technol.* **32** 270
[6] Stewart D K, Stern L A, Foss G, Hughes G and Govil P 1990 Focused ion beam induced tungsten deposition for repair of clear defects on x-ray masks *Proc. SPIE* **1263** 21
[7] Walker J F, Reiner J C and Solenthaler C 1995 Focused ion beam sample preparation for TEM *Proc. Microsc. Semicond. Mater. Conf. (Oxford, 20–23 March 1995)* p 629
[8] Athas G J, Noll K E, Mello R, Hill R, Yansen D, Wenners F F, Nadeau J P, Ngo T and Siebers M 1997 Focused ion beam system for automated MEMS prototyping and processing *Proc. SPIE* **3223** 198
[9] Daniel J H and Moore D F 1999 A microaccelerometer structure fabricated in silicon-on-insulator using a focused ion beam process *Sensors Actuators* A **73** 201
[10] Brugger J, Beljakovic G, Despont M, de Rooij N F and Vettiger P 1997 Silicon micro/nanomechanical device fabrication based on focused ion beam surface modification and KOH etching *Microelectron. Eng.* **35** 401
[11] Thornell G and Johansson S 1998 Microprocessing at the fingertips *J. Micromech. Microeng.* **8** 251
[12] Johansson S, Schweitz J-A, Westberg H and Boman M 1992 Microfabrication of three-dimensional boron structures by laser chemical processing *J. Appl. Phys.* **72** 5956
[13] Levin J P, Blauner P G and Wagner A 1990 Model for focused ion beam deposition *Proc. SPIE* **1263** 2
[14] Kubena R L and Stratton F P 1988 Selective area nucleation for metal chemical vapor deposition using focused ion beams *J. Vac. Sci. Technol.* B **6** 1865
[15] Blauner P G, Ro J S, Butt Y and Melngailis J 1989 Focused ion beam fabrication of submicron gold structures *J. Vac. Sci. Technol.* B **7** 609
[16] Bender H 2000 Ion beams focus on semiconductor devices *Vacuum Solutions* **1** 11
[17] Puers R, Vandevoorde G and De Bruyker D 2000 Electrodeposited copper inductors for intraocular pressure telemetry *J. Micromech. Microeng.* **10** 124
[18] Bienstman J, Vandewalle J and Puers R 1999 Synchronisation and collective behaviour in a network of non-linear resonators: a new approach to redundant sensing *Proc. Transducers 99* p 1398
[19] Metev S M and Veiko V P 1994 *Laser-Assisted Microtechnology* (Berlin: Springer)
[20] Monneret S, Loubère V and Corbel S 1999 Microstereolithography using a dynamic mask generator and a non-cohorent visible light source *Proc. Symp. on Design, Test and Microfabrication of MEMS and MOEMS (Paris, France)* p 553
[21] Miller J C (ed) 1994 *Laser Ablation, Principles and Applications* (Berlin: Springer)
[22] Song X, Reynaerts D, Meeusen W and Van Brussel H 1999 Investigation of micro-EDM for silicon microstructure fabrication *Proc. Symp. on Design, Test and Microfabrication of MEMS and MOEMS (Paris, France)* p 792
[23] Walker J F, Moore D F and Whitney J T 1996 Focused ion beam processing for microscale fabrication *Microelectron. Eng.* **30** 517
[24] Young R J 1993 Micro-machining using a focused ion beam *Vacuum* **44** 353
[25] Reyntjens S and Puers R 2000 Fabrication and testing of custom vacuum encapsulations deposited by focused ion beam direct-write CVD *Proc. Eurosensors XIV (Copenhagen, Denmark)* p 349

[26] Schmidt B, Bischoff L and Teichert J 1997 Writing FIB implantation and subsequent anisotropic wet chemical etching for fabrication of 3D structures in silicon *Sensors Actuators* A **61** 369
[27] Daniel J H 1999 *Micromachining Silicon for MEMS* (Cambridge: MTP D F Moore Trinity Hall)
[28] Young R, Van Cappellen E and Carleson P 1999 Proper sample preparation improves TEM performance *Test Meas. World* **19** 29–37
[29] Bogh A 1971 Ethylene diamine–pyrocatechol–water mixture shows etching anomaly in boron-doped silicon *J. Electrochem. Soc.* **118** 401
[30] Reyntjens S and Puers R 2000 Focused ion beam induced deposition: fabrication of three-dimensional microstructures and Young's modulus of the deposited material *J. Micromech. Microeng.* **10** 181–8
[31] Ziegler J F, Biersack J P and Littmark U 1985 *The Stopping Range of Ions in Solids* (New York: Pergamon)